NASA/TM-2000-210282

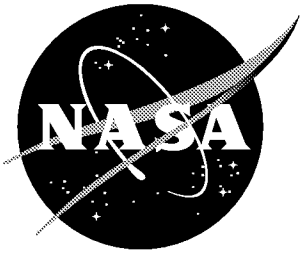

Prediction of Transonic Vortex Flows Using Linear and Nonlinear Turbulent Eddy Viscosity Models

Robert E. Bartels and Thomas B. Gatski
Langley Research Center, Hampton, Virginia

May 2000

The NASA STI Program Office ... in Profile

Since its founding, NASA has been dedicated to the advancement of aeronautics and space science. The NASA Scientific and Technical Information (STI) Program Office plays a key part in helping NASA maintain this important role.

The NASA STI Program Office is operated by Langley Research Center, the lead center for NASA's scientific and technical information. The NASA STI Program Office provides access to the NASA STI Database, the largest collection of aeronautical and space science STI in the world. The Program Office is also NASA's institutional mechanism for disseminating the results of its research and development activities. These results are published by NASA in the NASA STI Report Series, which includes the following report types:

- TECHNICAL PUBLICATION. Reports of completed research or a major significant phase of research that present the results of NASA programs and include extensive data or theoretical analysis. Includes compilations of significant scientific and technical data and information deemed to be of continuing reference value. NASA counterpart of peer-reviewed formal professional papers, but having less stringent limitations on manuscript length and extent of graphic presentations.

- TECHNICAL MEMORANDUM. Scientific and technical findings that are preliminary or of specialized interest, e.g., quick release reports, working papers, and bibliographies that contain minimal annotation. Does not contain extensive analysis.

- CONTRACTOR REPORT. Scientific and technical findings by NASA-sponsored contractors and grantees.

- CONFERENCE PUBLICATION. Collected papers from scientific and technical conferences, symposia, seminars, or other meetings sponsored or co-sponsored by NASA.

- SPECIAL PUBLICATION. Scientific, technical, or historical information from NASA programs, projects, and missions, often concerned with subjects having substantial public interest.

- TECHNICAL TRANSLATION. English-language translations of foreign scientific and technical material pertinent to NASA's mission.

Specialized services that complement the STI Program Office's diverse offerings include creating custom thesauri, building customized databases, organizing and publishing research results ... even providing videos.

For more information about the NASA STI Program Office, see the following:

- Access the NASA STI Program Home Page at ***http://www.sti.nasa.gov***

- E-mail your question via the Internet to help@sti.nasa.gov

- Fax your question to the NASA STI Help Desk at (301) 621-0134

- Phone the NASA STI Help Desk at (301) 621-0390

- Write to:
  NASA STI Help Desk
  NASA Center for AeroSpace Information
  7121 Standard Drive
  Hanover, MD 21076-1320

NASA/TM-2000-210282

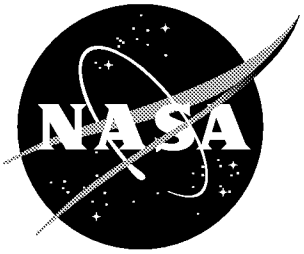

Prediction of Transonic Vortex Flows Using Linear and Nonlinear Turbulent Eddy Viscosity Models

Robert E. Bartels and Thomas B. Gatski
Langley Research Center, Hampton, Virginia

National Aeronautics and
Space Administration

Langley Research Center
Hampton, Virginia 23681-2199

May 2000

Available from:

NASA Center for AeroSpace Information (CASI)
7121 Standard Drive
Hanover, MD 21076-1320
(301) 621-0390

National Technical Information Service (NTIS)
5285 Port Royal Road
Springfield, VA 22161-2171
(703) 605-6000

Prediction of Transonic Vortex Flows Using Linear and Nonlinear Turbulent Eddy Viscosity Models

Robert E. Bartels and Thomas B. Gatski
NASA Langley Research Center
Hampton, VA 23681-0001

Abstract

Three-dimensional transonic flow over a delta wing is investigated with a focus on the effect of transition and influence of turbulence stress anisotropies. The performance of linear eddy viscosity models and an explicit algebraic stress model is assessed at the start of vortex flow, and the results compared with experimental data. To assess the effect of transition location, computations that either fix transition or are fully turbulent are performed. To assess the effect of the turbulent stress anisotropy, comparisons are made between predictions from the algebraic stress model and the linear eddy viscosity models. Both transition location and turbulent stress anisotropy significantly affect the 3D flow field. The most significant effect is found to be the modeling of transition location. At a Mach number of 0.90, the computed solution changes character from steady to unsteady depending on transition onset. Accounting for the anisotropies in the turbulent stresses also considerably impacts the flow, most notably in the outboard region of flow separation.

Nomenclature

C_f - Skin friction coefficient
C_m - Moment coefficient about pitch axis
C_N - Normal force coefficient
C_p - Pressure coefficient, $(p - p_\infty)/q_\infty$
M - Mach number
q_∞ - dynamic pressure
Re - Reynolds number based on root chord

Introduction

Turbulence models suitable for practical applications have been proposed ranging in complexity from the zero, one- and two-equation eddy viscosity models to full Reynolds stress closures. Among those, one- and two-equation models such as the k-ε or the k-ω shear stress transport (SST) models, solve transport equations for important physical parameters. Other transport models such as the Spalart-Allmaras (SA) are widely used although based more on empiricism. None of these model anisotropies in turbulent stresses. Anisotropic eddy-viscosity models have been developed to overcome this deficiency. Explicit algebraic stress models (EASMs), based on the initial work of Pope[1] and later generalized by Gatski and Speziale[2], are related to anisotropic eddy viscosity models, but depend on both rotational and irrotational strain rates. While the explicit algebraic stress model is a subset of the full Reynolds stress closure, it does retain a key feature of the full differential form by accounting for the Reynolds stress anisotropies that can occur in the flow. These anisotropies are reflected through the nonlinear terms in the tensor representation and directly affect the normal Reynolds stresses. In addition, the Reynolds shear stress is more accurately represented as well since the effective eddy viscosity is now directly sensitized to invariants associated with the mean strain rate and rotation rate tensors. Both these features distinguish the explicit algebraic model from the linear eddy viscosity class of models. Nevertheless, there are clearly many flows, which do not significantly deviate from the conditions

under which linear models have been optimized. In these flows the algebraic stress model, and the more general class of nonlinear eddy viscosity models, should not be expected to yield results significantly different than the lower-order linear eddy viscosity models.

This feature is borne out in the computational studies. Transition location has been found to impact relatively complex two-dimensional multi element airfoil flows,[3] although turbulent stress anisotropy did not appear to be a strong factor. Computations using an explicit algebraic stress model have been performed for several standard two- and three-dimensional wing cases. The authors of one study conclude that, while yielding results for those cases similar to those that would be obtained with the Johnson King turbulence model, an early version of the explicit algebraic stress model appeared to offer no advantages.[4] These applications most likely represent a class of flows for which linear eddy viscosity models have been optimized. To date, only in the cases of internal flow with strong curvature or complex three-dimensionality or involving shock/boundary layer interaction has an explicit algebraic stress model been demonstrated to offer a clear improvement over less complex models. It has been shown for an internal flow with strong curvature that an explicit algebraic stress model performs better than one- or two-equation eddy viscosity models and in some instances can produce results similar to a Reynolds stress model. [5,6] Rizzetta assessed the performance of three explicit algebraic Reynolds stress models for the two-dimensional shock separated flow over a supersonic compression ramp.[7] He found that while the Gatski-Speziale model produced better pressures and skin friction values than the other models, all models were deficient in accurately predicting stress anisotropies near the region of shock/boundary layer interaction. Sotiropoulos and Ventikas computed the three-dimensional flow through a curved duct.[8] They conclude that isotropic eddy viscosity models are inadequate for complex three-dimensional flows and that the explicit algebraic stress model of Gatski and Speziale offered some improvement.

Validation of an explicit algebraic stress model for an external strongly three-dimensional flow has not received much attention so far. An excellent, if challenging, candidate is the vortex flow over a delta wing. Experimental studies of delta wings have investigated a variety of phenomena and recently have offered detailed flow field turbulence budgeting.[9-11] Chow *et al.* have used triple-sensor hot wire probes to map the cross stream velocity field of a wing tip induced vortex.[11] The important result of their study is that Reynolds stress lags the strain rate with in the vortex. This necessitates a theoretical model that allows for anisotropic eddy viscosity. The performance of a delta wing is considerably dependent on whether the vortex has burst. For this reason, many experimental studies have focused on vortex breakdown. Gursul et al. have several studies attempting to characterize vortex unsteadiness induced by shedding, instability and breakdown.[12-13] Donohoe and Bannink have used surface reflective visualization to investigate vortex breakdown for a 65-deg sweep delta wing in high subsonic flow.[14] They found that the presence of a terminating shock-wave system interacting with the vortex significantly impacted the overall flow and can induce breakdown. They present visual data of interactions of the leading edge vortices with the very complex multiple shocks occurring at high subsonic speeds.

Computational investigations of delta wings have typically focused on geometric or flow modeling issues, or have attempted to simulate vortex development, instability or breakdown. Recent efforts have made use of the Euler equations[15-16,18] , laminar[17,18] and turbulent Navier-Stokes equations with zero- and one-equation turbulence models.[18-21] One study found that the primary vortex location and vorticity level over a delta wing are altered very little by viscous effects, although viscous solutions exhibited secondary and tertiary vortices not seen in the Euler solutions.[18] Another work points out that important flow details are obtained only by a viscous solution.[16] For example, significant flow separation over the wing can alter the vortex location. Turbulent transonic flow computations for another delta wing revealed little difference between

the Baldwin-Lomax and the Johnson-King turbulence models. [20] In another study of a similar delta wing, the Degani-Schiff and the Johnson-King models showed similar results,[16] while results with the Baldwin-Lomax model differed somewhat from the other two models.[16] It is clear at least that the non-equilibrium effects embodied in the Johnson-King model were not important in those cases. Yet one would expect that the isotropic eddy viscosity turbulence models used in the previous examples are not completely adequate for complex three-dimensional vortex delta wing flows. Whether or not the anisotropic eddy viscosity of an explicit algebraic eddy viscosity model will offer an improvement remains an open question. Having said this, it may be, as suggested, that grid resolution and other grid related issues are possibly of as much or more significance than turbulence model.[16]

Recent experimental studies using a simple straked delta wing are discussed in Refs. 22-24 and 34. A low speed test was initially performed and reported, followed by a transonic test. Out of that combined series of tests, a large body of pressure data, light sheet visualization and some particle image velocimetry data has been compiled for fixed and oscillating incidence wings at several Mach numbers over a range of incidences. The sectional and planform shapes of the low speed and transonic models were somewhat different. One key difference is a transition strip near the leading edge of the outboard panel of the transonic wing. This necessitates the use of turbulence modeling in the simulation of the transonic flow, but also allows an analysis of the turbulence model and transition location as separate effects. Published test results offer quite complex three-dimensional low speed and transonic flow fields. Although no detailed turbulence data has yet been published, pressure and visualization data from those tests reveal interesting phenomena such as self-induced shock/vortex oscillation and finger shocklets at certain incidences at very high subsonic speeds. Several computational studies have made use of the low speed data, [25-27] however, to date, no study has focused on the effect of the turbulence model and transition on the simulation of the transonic vortex flow. In the current study we have investigated the effect of turbulence model and transition location on the straked delta wing flow field at an incidence at which vortex flow begins. In particular, the explicit algebraic turbulence model of Gatski and Speziale is compared with several linear eddy viscosity models to study the effect of shear stress anisotropy on the flow field.

Method

The computer code CFL3D solves the three-dimensional thin-layer Reynolds averaged Navier-Stokes equations using an upwind finite volume formulation.[28] It is capable of solving multiple zone grids with one-to-one connectivity. Grid sequencing and local time stepping for convergence acceleration to a steady state are employed. Upwind-biased spatial differencing is used for the inviscid terms with flux limiting in the presence of shocks. The viscous terms are centrally differenced. Cross diffusion terms are neglected. The flux-difference splitting (FDS) method of Roe[29] is employed to obtain fluxes at cell faces. The turbulence models are solved uncoupled from the flow equations. Details of the SA and the SST turbulence models can be found in their respective references.[30,31] The form of the Gatski-Speziale EASM model used includes turbulence anisotropy effects. Additional details of the Gatski-Speziale k-ε EASM model and its implementation in CFL3D are discussed elsewhere.[5]

Results

The type of mesh used in the present problem has been dictated by the geometry. Mesh type is of considerable importance. The computation of the flow about a delta wing was used to show that the near apex suction peak of a developing inviscid vortex is better resolved with a conical mesh.

[32,33] Implementation of a conical or spherical mesh for a delta wing with simple geometry is straightforward. However, realistic aircraft configurations, with spanwise discontinuities due to strake-delta junction, with partial span leading and trailing edge surfaces or turbulence strips, complicate modeling, and can potentially require multi-block with several grid types, or worse, the use of a grid that is less than optimal for simulation of the vortex development. One approach is to use a chimera mesh. Another remedy used for a straked delta is a multi-block mesh. In this approach, the straked delta wing is embedded in a conical or spherical mesh while the remainder of the mesh has a C-H or O-H topology.[25] The difficulty in the problem presently under consideration is the need to model the partial span transition strip located at 14.5% behind the leading edge of the outer delta wing panel. In view of these obstacles a C-H grid is used here that is divided into multiple blocks. The combined surface grids for this wing are shown in Figures 1 and 2. An inboard span block covers the strake and all surface grid points down stream of the strake. The outboard span block covers all the wing surface grids outboard of the strake delta junction. In this way it is possible to turn on the turbulence production terms over the entire outboard delta wing panel aft of the grid line at the transition strip location. On the other hand, the convective and diffusive terms of the one- and two-equation turbulence models are included throughout the flow field.

Figure 2 presents the planform and experimental and computed pressure section locations. There are four chord wise sections on the outboard wing and three spanwise sections spanning the strake to outer wing panel. Most of the data in this report are for pressure coefficient at the spanwise and chord wise locations. The cases analyzed in references 22, 23 and 34 cover angles of attack from zero to beyond vortex bursting, at Mach numbers of 0.225, 0.60 and 0.90. Cunningham and Geurts find a dramatic shift in the character of the flow between the Mach numbers of 0.60 and 0.90.[34] The appearance of a shock at the high subsonic Mach number impacts both overall flow field development and the behavior of the force coefficients. Two of the most significant events at the higher Mach number are leading edge and shock induced trailing edge separations. These appear at an angle of attack at which vortex flow begins, and it is just these conditions that will be considered in the present report. As summarized in Table 1, the experimental data and computed solutions are at free stream Mach numbers of 0.60 and 0.90 and a Reynolds number of 8 million. Other than the important influences of Mach number and angle of attack, several key factors have been found to influence the present computational results. They are the grid, turbulent transition and turbulence model. The following sections discuss these important aspects in turn and their influence on the solutions at the two Mach numbers.

Grid sensitivity

In the present computations a moderately refined mesh has been used in most cases owing to the additional effort required for the turbulence models used here. This is called the standard grid. The multi-block standard grid is composed of 4 blocks, which if combined into a single mesh would comprise a C-H mesh with 153×65×57 grids in the stream wise, spanwise and normal directions. Wall spacing is 1×10^{-7} and 1×10^{-6} at the leading and trailing edges, respectively. The grid extends to 5.5 chord lengths away from the wing. For the purpose of assessing grid convergence, a fine grid has also been used. It has combined dimensions of 233×105×89 grids in the stream wise, spanwise and normal directions. This mesh is divided into six blocks. A medium and coarse grid were constructed by eliminating every other grid point from each of the blocks in the fine and medium grids.

A grid resolution study was conducted using the fine, medium and coarse grids, corresponding to cases 1-3 in Table 1. Initial computations with the fine grid modeling the transition location at the experimental location of 14.5% chord aft of the leading edge over the entire strake and delta wing

resulted in spatial oscillations in the section pressure distributions that did not match the experimental data. After several computations in which transition location was moved forward of the experimental location, a final computational transition location fixed at 6% chord was chosen, and is used in all of the computations that follow. For purposes of the grid resolution study 6% chord transition was used over the entire strake delta wing. As will be discussed in the next section, all other computations modeling transition with the standard grid included a large region of laminar flow over the strake.

A survey of the results in Table 1 for cases 1-6, show that the computed force coefficients at a Mach number of 0.60, using the fine and the standard grids, matched the experimental values quite well. This is in contrast to the computed force coefficients at a Mach number of 0.90 using the standard mesh, for which the moment coefficient in each case was less than half the experimental value. The difficulty in matching moment coefficient at this Mach number is probably due to the fact that there is a significant amount of shock-induced separation.

Figures 3-4 present the pressure distributions resulting from the grid resolution study. At each pressure section, the trend with successive refinement of the grid is to match more closely the experimental data. The pressure peaks shown in sections 1, 5 and 6 are due to the strake and wing vortex development. The wing vortex in the early stages of development is tightly bound, as seen in the very sharply focused pressure peaks of sections 1 and 6. The finest mesh better captures the confinement of the wing vortex in the early stages of development, although it is not adequately simulated by any of the grids. However, down stream developments of the wing and strake vortices are captured quite well by the fine mesh. This can be seen in the pressure peaks of section 7. An important feature to notice is that vortex location is sensitive to grid resolution. Both the strength and location of the strake and wing vortices are better simulated with the more refined grid. This is clearly exemplified by the pressures of section 7, where both the wing and strake vortex locations and strengths are reproduced quite well with the fine grid. This is also clearly indicated in section 5 where the fine mesh reproduces the early strake vortex strength and location very well. In general, the conclusion of this grid study is that while even the fine mesh does not adequately resolve several portions of the flow field, much of the flow field is modeled quite well by the finest mesh. The standard grid used in all of the remaining computations represents a resolution that is between that of the medium and fine grids.

Effect of transition

Computations using the standard grid with several combinations of transition from fully turbulent to transition outboard with largely laminar strake panel were performed. Fully turbulent computations included turbulence production terms throughout the flow field. The computations including the effect of the partial span transition strip were accomplished via multi-block as discussed earlier. A transition strip on the outer panel was modeled in most of the computations by turning off turbulence production terms forward of 6% chord. Other than for the grid resolution study and the computations that were fully turbulent, the strake region was computed with the turbulence production terms turned on at the 95% chord location. The location of 95% was chosen after computations using the standard grid with transition located at the leading edge, 72% and 95% chord. This last transition location for the inboard panel resulted in the best match with the experimental data at a Mach number of 0.90. Furthermore, the computations in which transition was at the leading edge (case number 8) and at 72% chord reached a steady state, while the solution at 95% (case number 11) resulted in a limit cycle oscillatory solution. This aspect of the solution will be discussed subsequently.

Considering the results of cases 7-11, summarized in Table 1, it can be concluded that the modeling of transition significantly improves the comparison of force and moment coefficients with experiment. The data of Figures 5 and 6 at an angle of attack of 9.38 degrees are presented for comparison with the results at an angle of attack of 11.39 degrees in Figures 9 and 10. The experimental data show a change in character from quasi steady at 9.38 degrees to unsteady limit cycle oscillation of the shock and vortices at an angle of attack of 11.39 degrees.[34] This shift in the nature of the solution has also been captured in the present computations. The solution at 9.38 degrees and a Mach number of 0.90, which includes the modeling of transition, reached a fully steady state. This solution is shown in Figures 5 and 6. The solution with identical transition and turbulence modeling, at 11.94 degrees and a Mach number of 0.60 also reached a steady state. All of the fully turbulent solutions at 11.39 degrees, shown in Figures 7 and 8, also reached a steady state.

The results of a solution at 11.39 degrees angle of attack, modeling transition with the SA model, are shown in Figures 9 and 10. This solution reached an unsteady limit cycle oscillation. The mean, minimum and maximum pressures distributed over the seven sections shown in Figures 9 and 10, show that transition modeling does significantly improve the computed pressure distributions relative to experiment compared to the fully turbulent steady computations shown in Figures 7 and 8. This effect is most noticeable at sections 1, 3,4 and 7. These results also indicate that the unsteadiness in the computed solution is almost entirely confined to the strake panel region. Cunningham and Geurts discuss the limit cycle oscillation of the flow field at this angle of attack.[34] They point out that the experimental unsteadiness appears to be mostly outboard of and including section 1. In this respect the unsteadiness in the computed solution does not match the experiment.

Effect of turbulence model

Figures 11-12 present computed pressure distributions corresponding to cases 4-6 in Table 1. In these cases transition is modeled. Computed results using the explicit algebraic stress model of Gatski and Speziale[2] (EASM), the Spalart-Allmaras model (SA), the k-ω shear stress transport model (SST) are compared with experiment. At a Mach number of 0.60 compressibility and transonic effects can be expected to be just beginning to influence the flow field. The effect of the transonic shock and shock separation (SITES – shock induced trailing edge separation) apparent at Mach number of 0.90 do not yet appear in the pressure distributions at this Mach number. At a Mach number of 0.60 (Figures 11-12), the pressure distributions produced by all of the turbulence models fairly accurately reproduce the experimental data. The pressure sections 1 and 2 in Figure 11 are the locations at which the most noticeable differences in turbulence model appear, although it is unclear which model best reproduces the data. At section 1 the SA model offers a somewhat better match with the experimental data, although at section 2 the EASM model more accurately reproduces vortex strength and/or location. This region of the flow field clearly requires better grid resolution.

In contrast to the flow field at the lower Mach number, clear evidence of a shock is seen in the pressures distributions of Figures 7 and 8 at a Mach number of 0.90, including the effect of SITES and leading edge separation. Cases 8-11 from Table 1 are at a Mach number of 0.90. At this Mach number there is a more pronounced difference among turbulence models. Among the fully turbulent force and moment coefficient results, the EASM model most closely matches experiment. Figures 7 and 8 show that the EASM model offers improved pressure distributions in comparison with experiment at sections 2-4 and 7. These sections are in the outboard and trailing edge regions of the wing. As will be seen, these are areas in which there are large three-dimensional regions of boundary layer separation. The remaining pressure distributions in

Figures 13 and 14 compare the fully turbulent EASM steady pressures with the SA mean pressures modeling transition at the higher Mach number. Results for the outboard sections 3 and 4 show that the fully turbulent EASM model offers additional improvement over the SA results that had been improved by including transition. A solution was also computed with the EASM model that includes the effect of leading edge transition and the largely laminar strake region. This solution was unsteady although it was not possible to reach a fully converged limit cycle solution due to the computer time required. Instantaneous pressure distributions resulting from this solution are shown in Figures 15 and 16. In some regions this solution appears promising. The comparison of the pressure distribution at section 7 with experiment is excellent over all but the strake region and much improved in comparison with Figure 14. The pressures at sections 2, 3 and 4 are also in excellent agreement with experiment over most of the chord length. The puzzling excursions in the computed pressures may have been due to an extremely slowly converging solution, although that can only be conjectured from the results obtained.

Analysis of computed flow field

Figures 17-19 present experimental and computed flow field visualizations at laser light sheet locations 8 and 9 at Mach numbers of 0.60 and 0.90. The computed contours are for pressure coefficient. Pressure coefficient contours should best match the laser light sheet visualizations since water vapor is expected to condense in the supersonic stream and move toward regions of minimum pressure. The accumulation of water vapor gives the dark regions in the negative images. Each of the turbulence models at both Mach numbers gave strake and delta wing vortex locations that are relatively close in location to experiment. At a Mach number of 0.60 there is little difference between the turbulence models, and both show vortex locations quite close to that of experiment. At a Mach number of 0.90, the development of strake vortex is clearly seen to occur between 9.38 and 11.39 degrees angle of attack. (Figures 18 and 19) There are also clear differences evident between the turbulence models and between the fully turbulent and transitioned results. One striking difference is that the vortex core is not as focused when transition is modeled. This can be observed in the spreading and weakening of the minimum in pressure in the transition modeled results compared with those that are fully turbulent. Strengthening and expanding of the pressure minimum is evident as the angle of attack changes from 9.38 to 11.39 degrees. This can be seen in the experimental light sheets by comparing Figures 18 and 19 and coincides with the onset of vortex flow. An interesting feature also seen in the experimental laser light sheet image of Figure 19 is the vapor trail spreading from the strake vortex outboard toward the wing vortex. This feature is discussed at length by Cunningham and Geurts.[34] They suggest that this "gull wing" pattern is due to a shear layer interface between the "outer flows which see the spanwise flow potential propagating from the inboard strake region, and an inner supersonic flow near the wing surface." (p. 40) In Figure 20, computed spanwise velocity contours at laser light sheet 9 confirm the presence of a spanwise shear layer between the strake vortex and the wing vortex, where, however, the computed outer flow is directed inboard.

Figure 21 presents skin friction contours (negative skin friction appearing in darker shades) computed with the different turbulence models at Mach number 0.90 and 11.39 angle of attack. The SA model data computed with transition are instantaneous values. Leading edge separation appears experimentally just below 11 degrees while SITES appears between 10.4-10.5 degrees.[34] Both the leading and trailing edge separations and the shock-induced separation on the inboard section are revealed in all of the results. The extent and depth of the reversed flow regions computed with the anisotropic eddy viscosity model is much different than that computed by any of the linear eddy viscosity models. The extent of the in board shock separation is much smaller in the EASM results in comparison to the linear eddy viscosity results. The strength of the reversed flow in the leading edge area of the outboard wing is also much stronger in the EASM

results. This is evident in the skin friction (at pressure section 3), shown in Figure 22. This is the region in which the EASM model consistently produced better pressure distributions with respect to the experimental values compared with the linear eddy viscosity models. The skin friction distributions produced by the linear eddy viscosity models generally group together while the skin friction produced by the nonlinear eddy viscosity model is distinctly different over the entire chord length.

Conclusions

A computational study of the effect of grid resolution, turbulent transition location and anisotropy of turbulent stresses has been performed at transonic Mach numbers of 0.60 and 0.90 using the transonic straked delta wing. This study has shown that all three effects play important but different roles. Grid resolution has been found to be important at the lower Mach number. It is expected that it will be important at any Mach number since, proper development of the strake and wing vortices requires adequate grid resolution. Down stream vortex development of the solution with the finest grid, and in areas away from the vortex, however, appeared to match experiment very well at the lower Mach number. The simulation of transition location has a very strong effect on the resulting pressure distribution for the straked delta wing at a high subsonic Mach number at the start of vortex flow. The effect of transition is less evident but not completely insignificant at the low transonic Mach number as well. With respect to force coefficients, all turbulence models match well at the lower Mach number, while at the high subsonic Mach number, all are significantly off in moment. This is likely due to the fact that leading and shock induced trailing edge separation are key effects at the high subsonic Mach number at the start of vortex flow. However, with regard to force coefficients, several points can be made. Transition appears as an important contributor, in that the SA model with transition and laminar inboard section yields a moment coefficient closer to experiment than does the fully turbulent simulation with the same model. The fully turbulent EASM results also yielded significant improvement in moment coefficient at the higher Mach number. This would be expected if the outboard leading edge and in board shock separations include significant Reynolds stress anisotropies. With regard to pressure distributions, the fully turbulent field using the EASM model gives somewhat better pressures in the wing tip region at the higher Mach number. Even greater improvement is seen in the EASM results that include the effect of transition, although the reason for isolated anomalous excursions in pressures has yet to be resolved. At the high subsonic Mach number, the computed flow field simulation that included transition strip location and laminar strake flow has resulted in a limit cycle flow oscillation, whereas the fully turbulent computations with all the turbulence models reached a steady state solution. This coincides with the onset of unsteadiness in the experimental data. Although this is encouraging, the computed region of unsteadiness differs from the experiment. Further investigations are needed to more accurately reproduce the experimental phenomena observed. Otherwise, several aspects of the experimental data were reproduced well by the computations. The onset of vortex flow was computed well by all the turbulence models. The existence of the postulated spanwise shear layer between the strake and delta wing vortices was also confirmed by the present computations.

References

1. Pope, S. B., "A more general effective-viscosity hypothesis," *Journal of Fluid Mechanics*, Vol. 72, part 2, 1975, pp. 331-340.

2. Gatski, T. B. and Speziale, C. G., "On explicit algebraic stress models for complex turbulent flows," *Journal of Fluid Mechanics*, vol. 254, 1993, pp. 59-78.
3. Rumsey, C. L., Gatski, T. B., Ying, S. X. and Bertelrud, A., "Prediction of High-Lift Flows Using Turbulent Closure Models," *AIAA Journal*, Vol. 36, No. 5, May 1998, pp. 765-774.
4. Abid, R., Morrison, J. H., Gatski, T. B. and Speziale, C. G., "Prediction of Aerodynamic Flows with a New Explicit Algebraic Stress Model," *AIAA Journal*, Vol. 34, No. 12, December 1997, pp. 2632-2635.
5. Rumsey, C. L., Gatski, T. B., and Morrison, J. H., "Turbulence Model Predictions of Extra-Strain Rate Effects in Strongly-Curved Flows," AIAA paper 99-0157, *37th Aerospace Sciences Meeting and Exhibit,* January 11-14, 1999, Reno, NV.
6. Jongen, T., Mompean, G., Gatski, T. B., "Predicting S-Duct Flow Using a Composite Algebraic Stress Model," *AIAA Journal*, Vol. 36, No. 3, March 1998, pp. 327-335.
7. Rizzetta, D. P., "Evaluation of Explicit Algebraic Reynolds-Stress Models for Separated Supersonic Flows," *AIAA Journal*, Vol. 36, No. 1, January 1998, pp. 24-30.
8. Sotiropoulos, F. and Ventikos, Y., "Flow Through a Curved Duct Using Nonlinear Two-Equation Turbulence Models," *AIAA Journal*, Vol. 36, No. 7, July 1998, pp. 1256-1262.
9. Shah, P. N., Atsavapranee, P., Hsu, T. Y., Wei, T. and McHugh, J., "Turbulent transport in the core of a trailing edge half-delta-wing vortex," *Journal of Fluid Mechanics*, vol. 387, 1999, pp. 151-175.
10. Breitsamter, C. and Laschka, B., "Turbulent Flow Structure Associated with Vortex-Induced Fin Buffeting," *Journal of Aircraft*, Vol. 31, No. 4, July-Aug. 1994, pp. 773-781.
11. Chow, J. S., Zilliac, G. G. and Bradshaw, P., "Mean and Turbulence Measurements in the Near Field of a Wingtip Vortex," *AIAA Journal*, Vol. 35, No. 10, October 1997, pp. 1561-1567.
12. Gursul, I. and Xie, W., "Buffeting Flows over Delta Wings," *AIAA Journal*, Vol. 37, No. 1, January 1999, pp. 58-65.
13. Menke, M. and Gursul, I., "Unsteady nature of leading edge vortices," *Physics of Fluids*, Vol. 9, No. 10, October 1997, pp. 2960-2966.
14. Donohoe, S. R. and Bannink W. J., "Surface Reflective Visualizations of Shock-Wave/Vortex Interactions Above a Delta Wing," *AIAA Journal*, Vol. 35, No. 10, October 1997, pp. 1568-1573.
15. Hoeijmakers, H. W. M., Jacobs, J. M. J. W., van den Berg, J. I., "Numerical Simulation of Vortical Flow over a Delta Wing at Subsonic and Transonic Speeds," NLR TP-90029, September 1990.
16. Longo, J. M. A., "Simulation of Complex Inviscid and Viscous Vortex Flow," *Fluid Dynamics of High Angle Attack,* IUTAM Symposium Tokyo, Japan, September 13-17, 1992, Kawamura, R., Aihara, Y., eds..
17. Gordnier, R. E., "Numerical Simulation of a 65-Degree Delta-Wing Flowfield," *Journal of Aircraft*, Vol. 34, No. 4, July-August 1997, pp. 492-499.
18. Agrawal, S., Barnett, R. M., Robinson, B. A., "Numerical Investigation of Vortex Breakdown on a Delta Wing," *AIAA Journal*, Vol. 30, No. 3, March 1992, pp. 584-591.
19. Tuncer, I. H. and Platzer, M. F., "Computational Study of Subsonic Flow over a Delta Canard-Wing-Body Configuration," *Journal of Aircraft*, Vol. 35, No. 4, July-August 1998, pp. 554- 560.
20. Kaynak, U., Tu, E., Dindar, M. and Barlas, R., "Nonequilibrium Turbulence Modeling Effects on Transonic Vortical Flows about Delta Wings," AGARD CP-494, *Vortex Flow Aerodynamics*, July 1, 1991.
21. Ekaterinaris, J. A. and Schiff, L. B., "Vortical Flows over Delta Wings and Numerical Prediction of Vortex Breakdown," AIAA-90-0102, 28th Aerospace Sciences Meeting, January 8-11, 1990, Reno, NV.

22. Cunningham, A. M., den Boer, R. G., Dogger, C. S. G., Geurts, E. G. M., Retel, A. P. and Zwaan, R. J., "Unsteady Transonic Wind Tunnel Test on a Semi span Straked Delta Wing Model Oscillating in Pitch, Part 1: Description of Model, Test Setup, Data Acquisition and Data Processing," Wright Laboratory report WL-TR-94-3094, December 1994.
23. Cunningham, A. M. and Geurts, E. G. M., "Analysis of Limit Cycle Oscillation/Transonic High Alpha Flow Visualization, Part 2: Stationary Model Data," Air Force Research Laboratory report AFRL-VA-WP-TR-1998-3004, January 1998.
24. Cunningham, A. M. and den Boer, R. G., "Low-Speed Unsteady Aerodynamics of a Pitching Strake Wing at High Incidence-Part II: Harmonic analysis," *Journal of Aircraft*, Vol. 27, No. 1, January 1990, pp. 31-41.
25. Kern, S. B., "Numerical Investigation of Vortex Flow Control Through Small Geometry Modifications at the Strake/Wing Junction of a Cropped Double Delta Wing," AIAA-92-0411, 30th Aerospace Sciences Meeting and Exhibit, January 6-9, 1992, Reno, NV.
26. Ekaterinaris, J. A., Coutley, R. L., Schiff, L. B., Platzer, M. F., "Numerical Investigation of the Flow over a Double Delta Wing at High Incidence," AIAA-91-0753, 29th Aerospace Sciences Meeting, January 7-10, 1991, Reno NV.
27. Ekaterinaris, J. A. and Schiff, L. B., "Navier-Stokes Solutions for an Oscillating Double-Delta Wing," AIAA-91-1624, AIAA 22nd Fluid Dynamics, Plasma Dynamics and Lasers Conference, June 24-26, 1991, Honolulu, Hawaii.
28. Krist, S. L., Biedron, R. T., and Rumsey C. L., "CFL3D User's Manual (Version 5.0)," NASA TM-1998-208444, June 1998.
29. Roe, P. L., "Approximate Riemann Solvers, Parameter Vectors, and Difference Schemes," *Journal of Computational Physics*, Vol. 43, 1981, pp. 357-372.
30. Spalart, P. R., and Allmaras, S. R., "A One-Equation Turbulence Model for Aerodynamic Flows," *La Recherche Aerospatiale*, No. 1, 1994, pp. 5-21.
31. Menter, F. R., "Improved Two-Equation k-ω Turbulence Models for Aerodynamic Flows," NASA TM 103975, Oct. 1992.
32. Kumar, A., "Role of flow-consistent grid in CFD," *Computers and Fluids*, Vol. 28, 1999, pp. 265-280.
33. Kumar, A., and Sudharsan, R., "Computation of Vortex Flow on a Delta Wing Using a Multi-Block Grid," *Computational Fluid Dynamics Journal*, Vol. 4, No. 1, 1995, pp. 99-112.
34. Cunningham, A. M., Geurts, E. G. M., "Analysis of Limit Cycle Oscillation/Transonic High Alpha Flow Visualization, Part 1: Discussion, Air Force Research Laboratory Report AFRL-VA-WP-TR-1998-3003, January 1998.

Table 1. Case data

Case No.	M_∞	α (Deg.)	C_N (Calc.)	C_N (Exp.)	C_m (Calc.)	C_m (Exp.)	Comp. Flow Type	Turb. Model & Transition	Grid
1	0.601	11.94	0.680	0.65	0.0231	0.030	steady	SA (trans)	coarse
2	0.601	11.94	0.663	0.65	0.0275	0.030	steady	SA (trans)	medium
3	0.601	11.94	0.647	0.65	0.0292	0.030	steady	SA (trans)	fine
4	0.601	11.94	0.650	0.65	0.0281	0.030	steady	SA (trans)	standard
5	0.601	11.94	0.656	0.65	0.0300	0.030	steady	SST (trans)	standard
6	0.601	11.94	0.640	0.65	0.0280	0.030	steady	EASM (trans)	standard
7	0.900	9.38	0.594	0.64	0.00164	0.005	steady	SA (trans)	standard
8	0.899	11.39	0.720	0.69	0.00228	0.013	steady	SA (full turb)	standard
9	0.899	11.39	0.709	0.69	0.00378	0.013	steady	SST (full turb)	standard
10	0.899	11.39	0.697	0.69	0.00533	0.013	steady	EASM (full turb)	standard
11	0.899	11.39	0.690 ‡	0.69	0.00589 ‡	0.013	unstdy	SA (trans)	standard

‡ Mean value

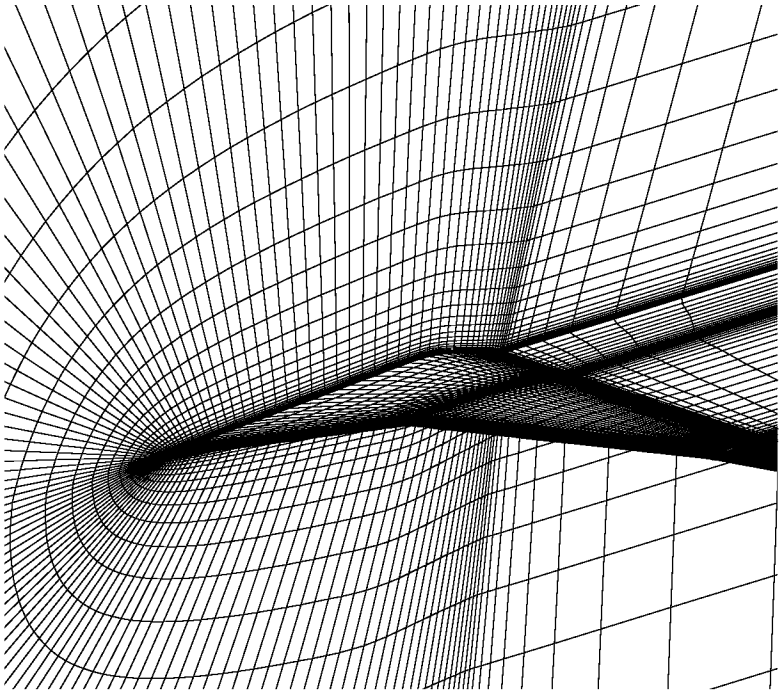

Figure 1. Straked delta wing C-H grid boundaries (standard grid).

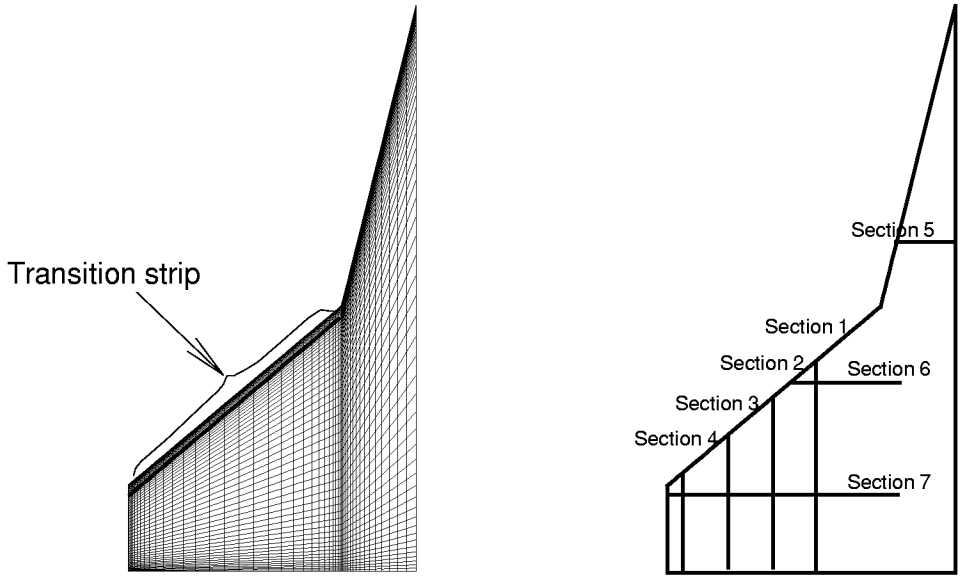

Figure 2. Surface grids (standard grid) and pressure section layout.

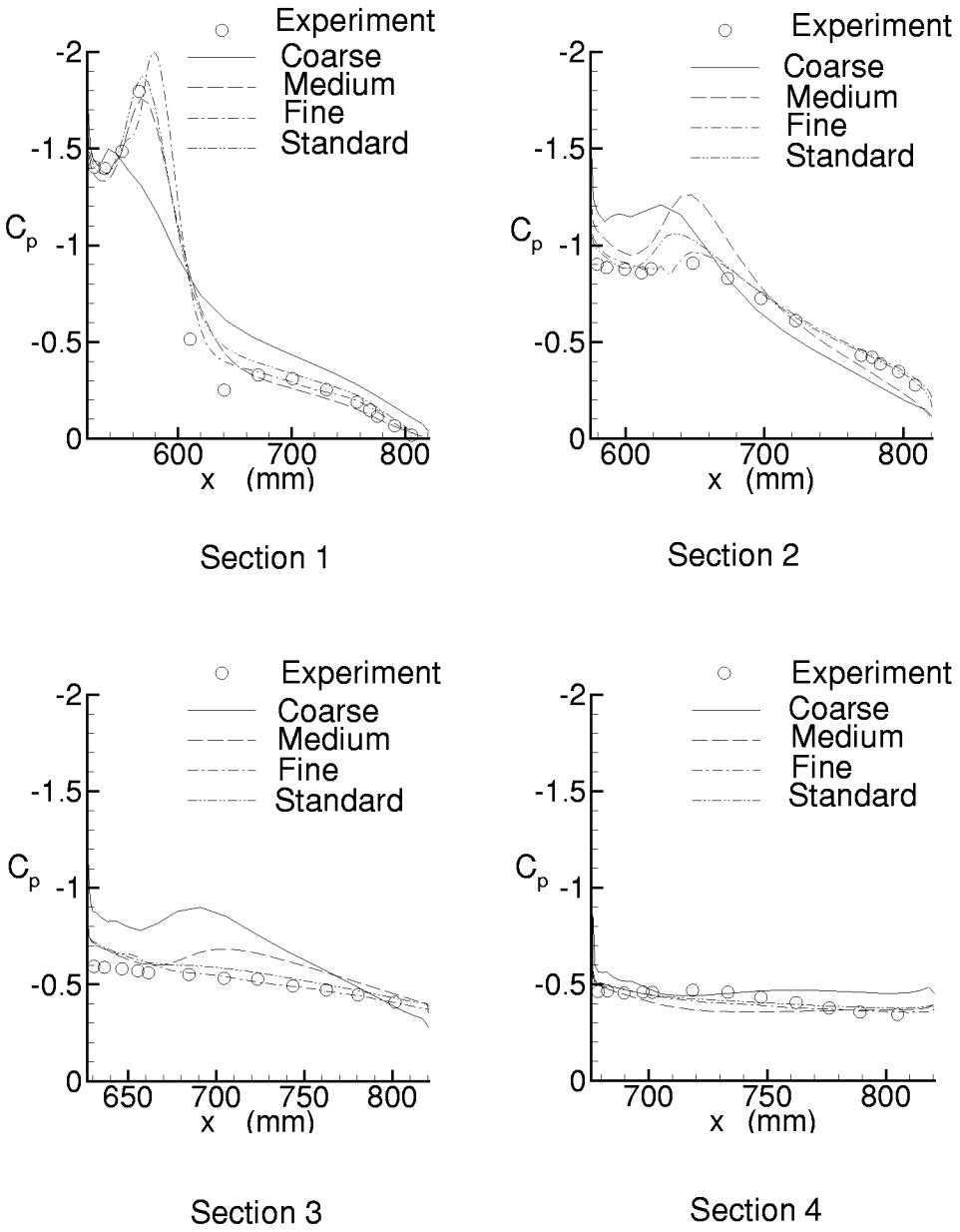

Figure 3. Chord wise pressure coefficient distributions at span sections. M = 0.601, α = 11.94 degrees, Re = 8 million. Transition modeled.

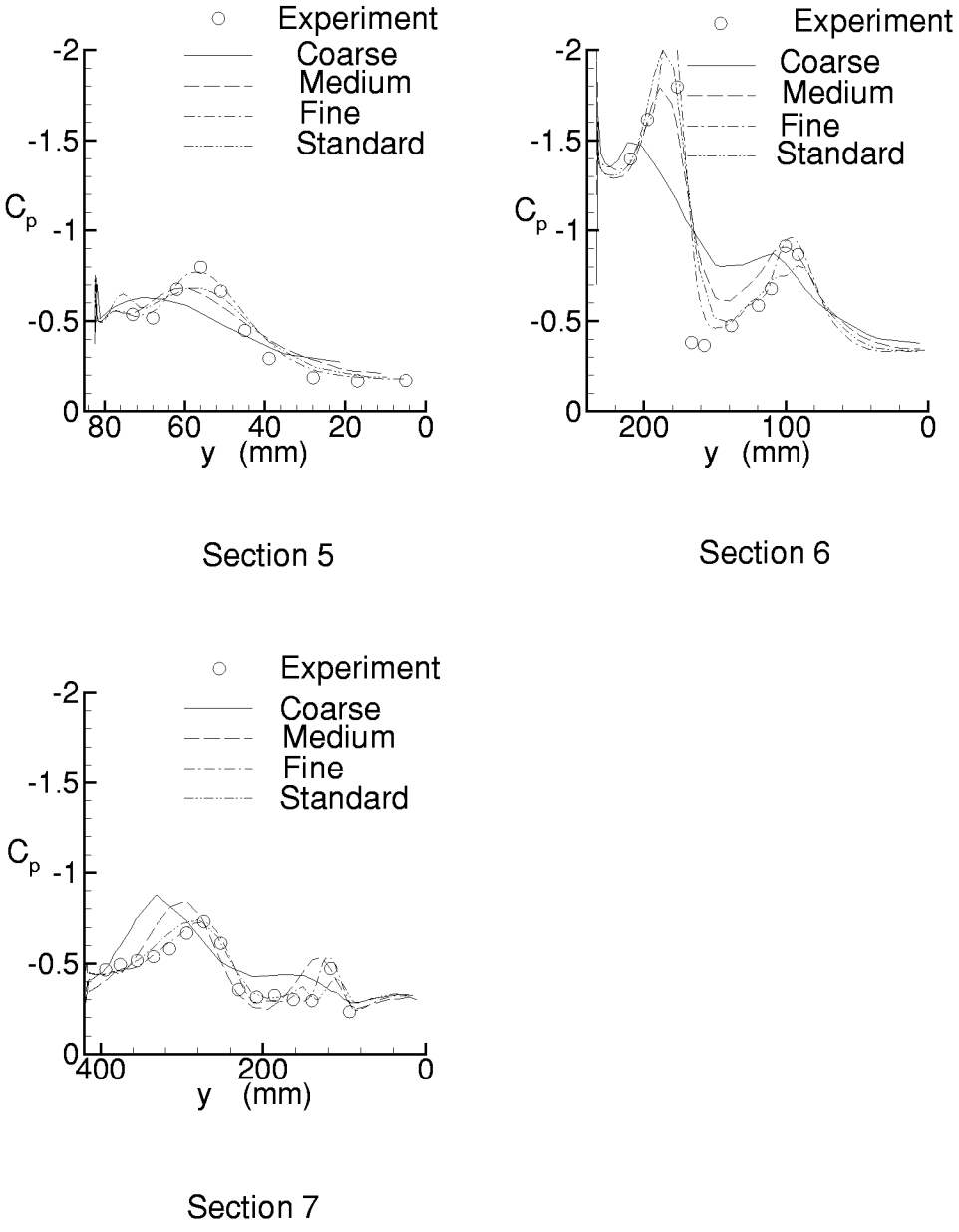

Figure 4. Spanwise pressure coefficient distributions at chord sections. M = 0.601, α = 11.94 degrees, Re = 8 million. Transition modeled.

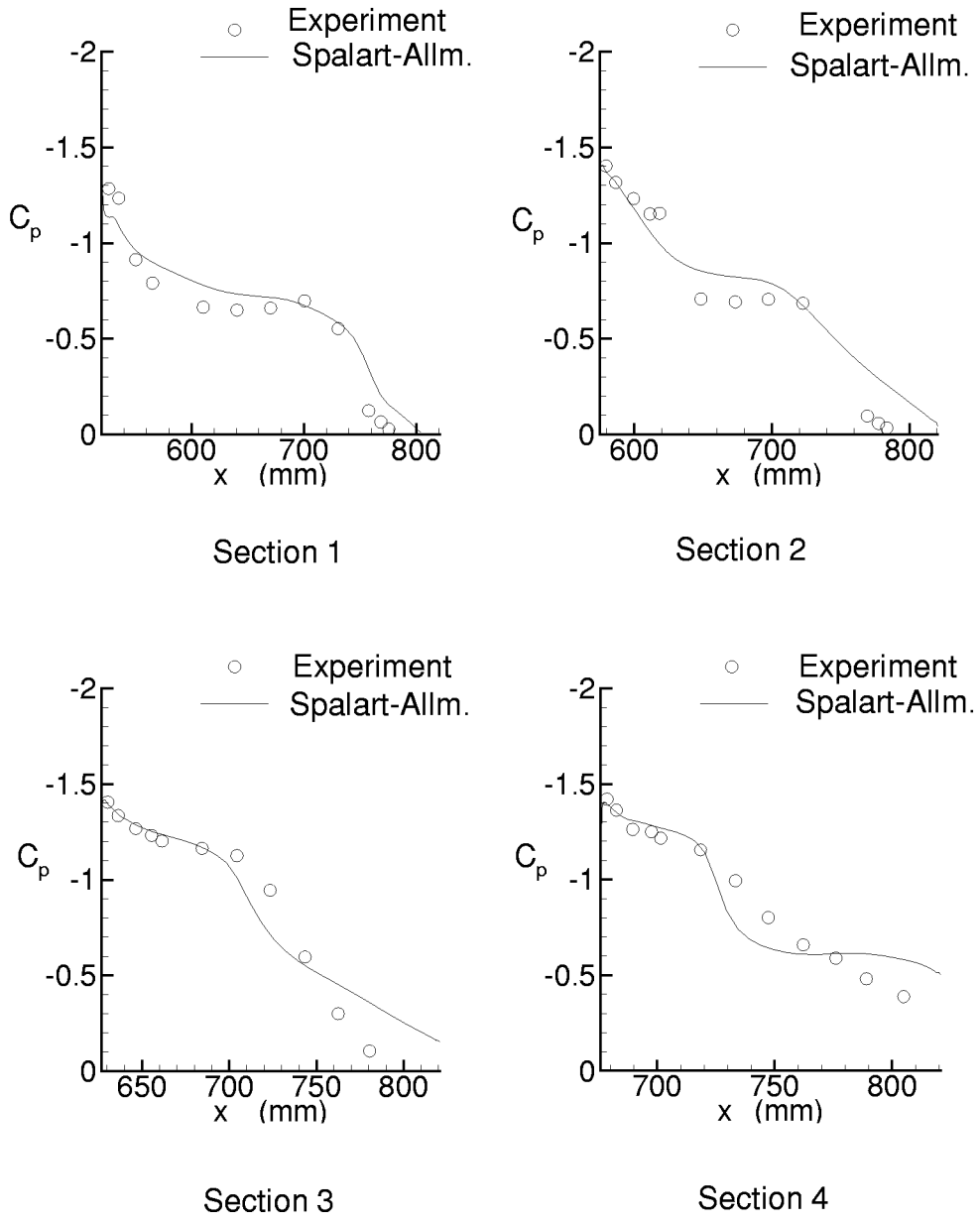

Figure 5. Chord wise pressure coefficient distributions at span sections. M = 0.900, α = 9.38 degrees, Re = 8 million. Transition modeled.

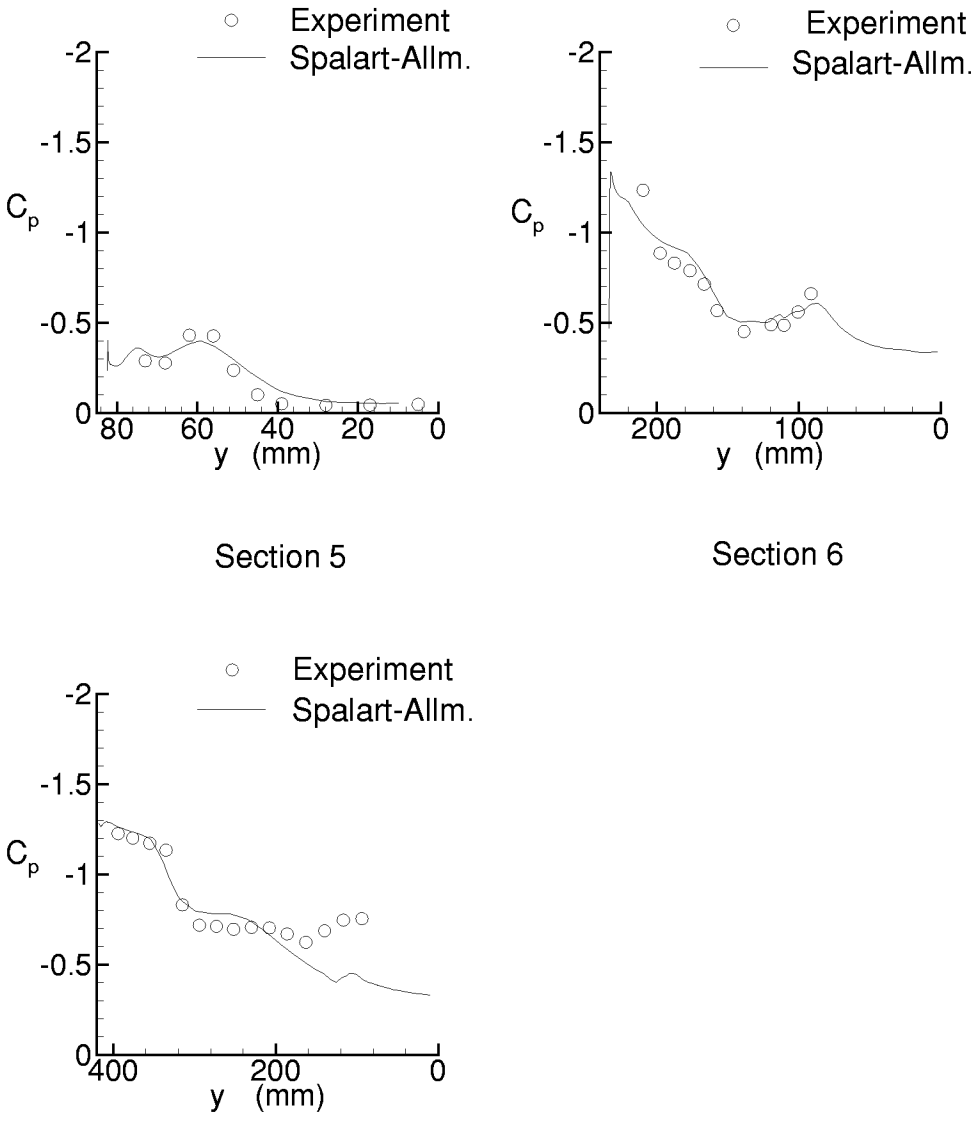

Figure 6. Chord wise pressure coefficient distributions at span sections. M = 0.900, α = 9.38 degrees, Re = 8 million. Transition modeled.

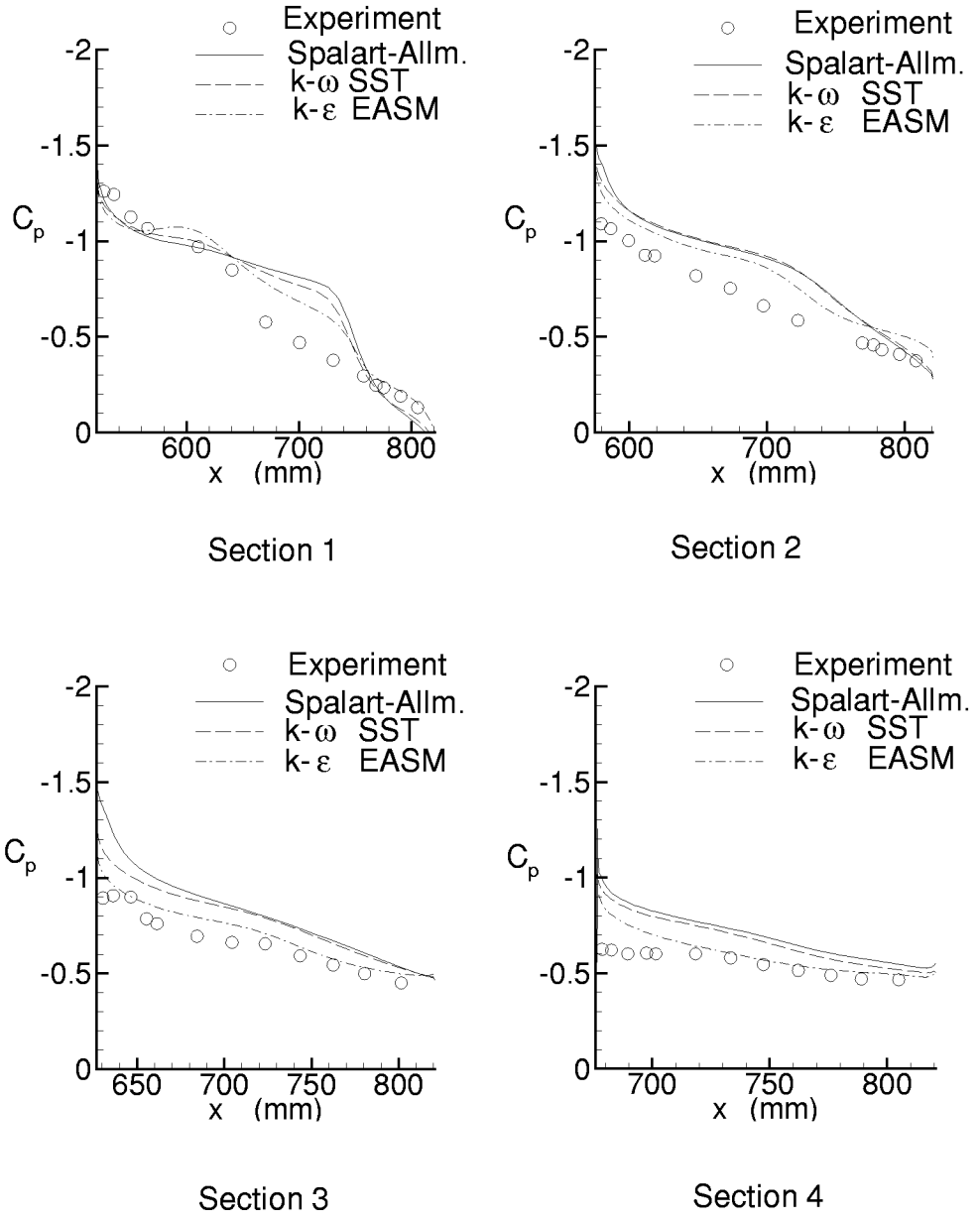

Figure 7. Chord wise pressure coefficient distributions at span sections. M = 0.899, α = 11.39 degrees, Re = 8 million. Fully turbulent.

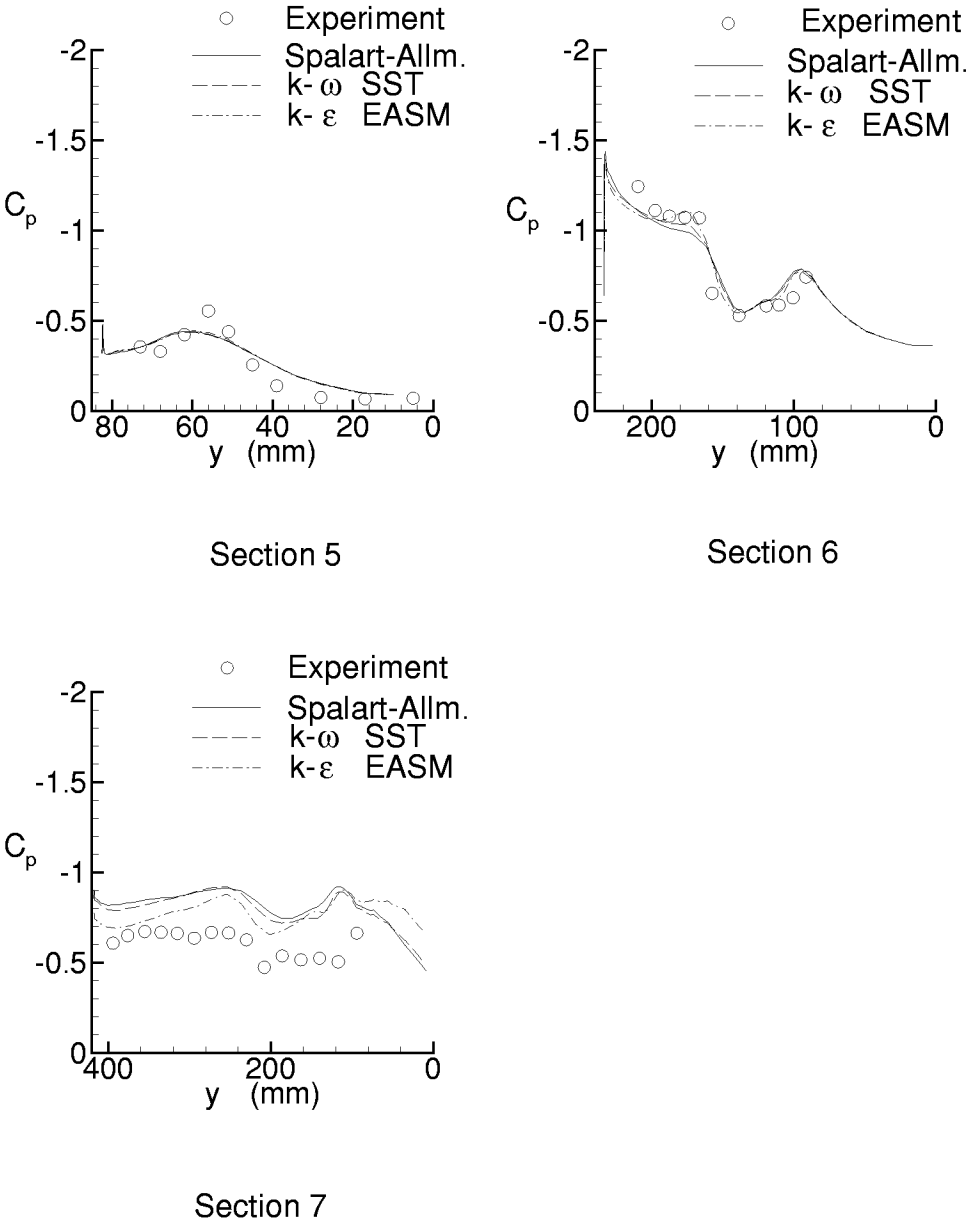

Figure 8. Spanwise pressure coefficient distributions at chord sections. M = 0.899, α = 11.39 degrees, Re = 8 million. Fully turbulent.

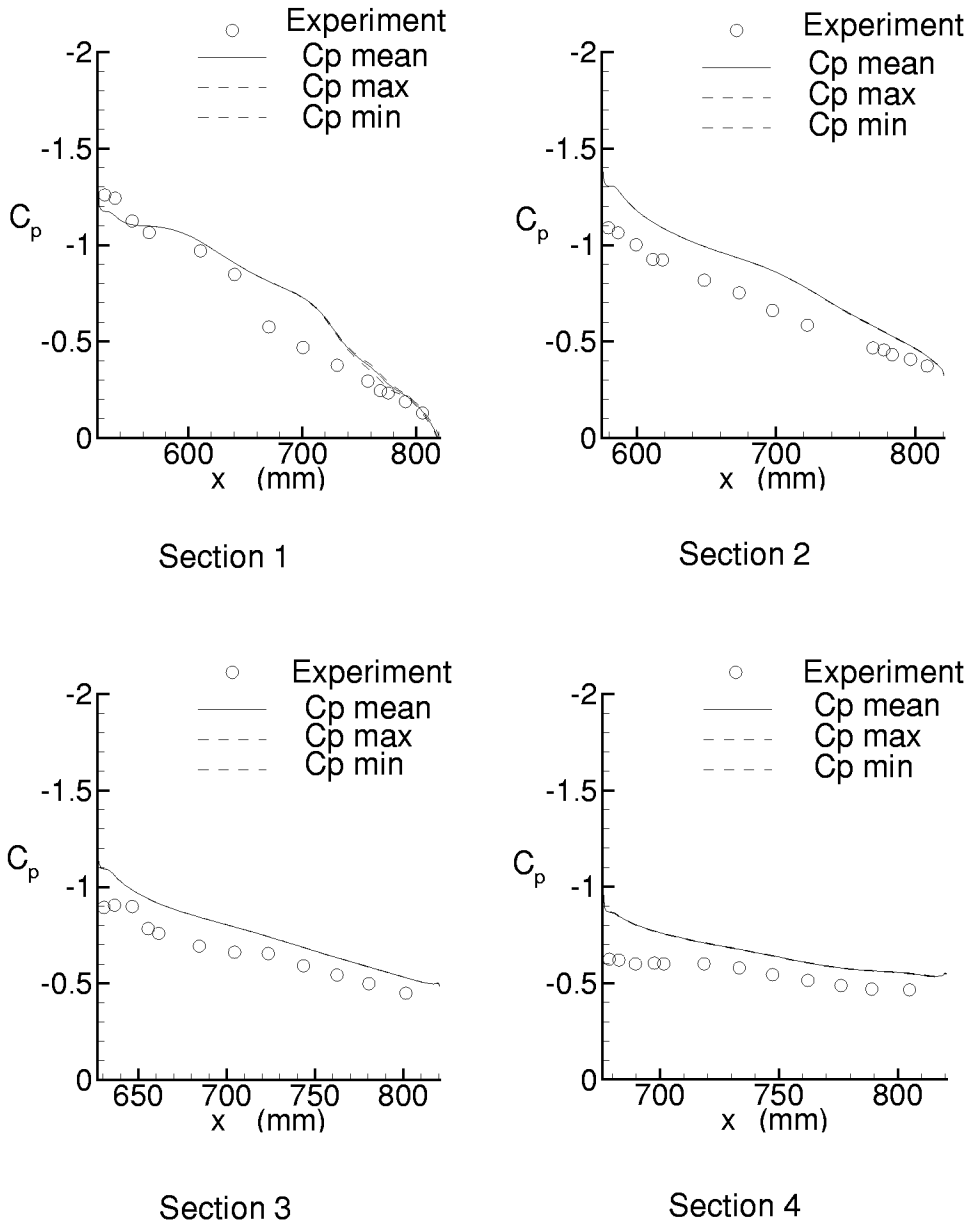

Figure 9. Chord wise unsteady pressure coefficient distributions at span sections. M = 0.899, α = 11.39 degrees, Re = 8 million. Spalart-Allmaras model. Transition modeled.

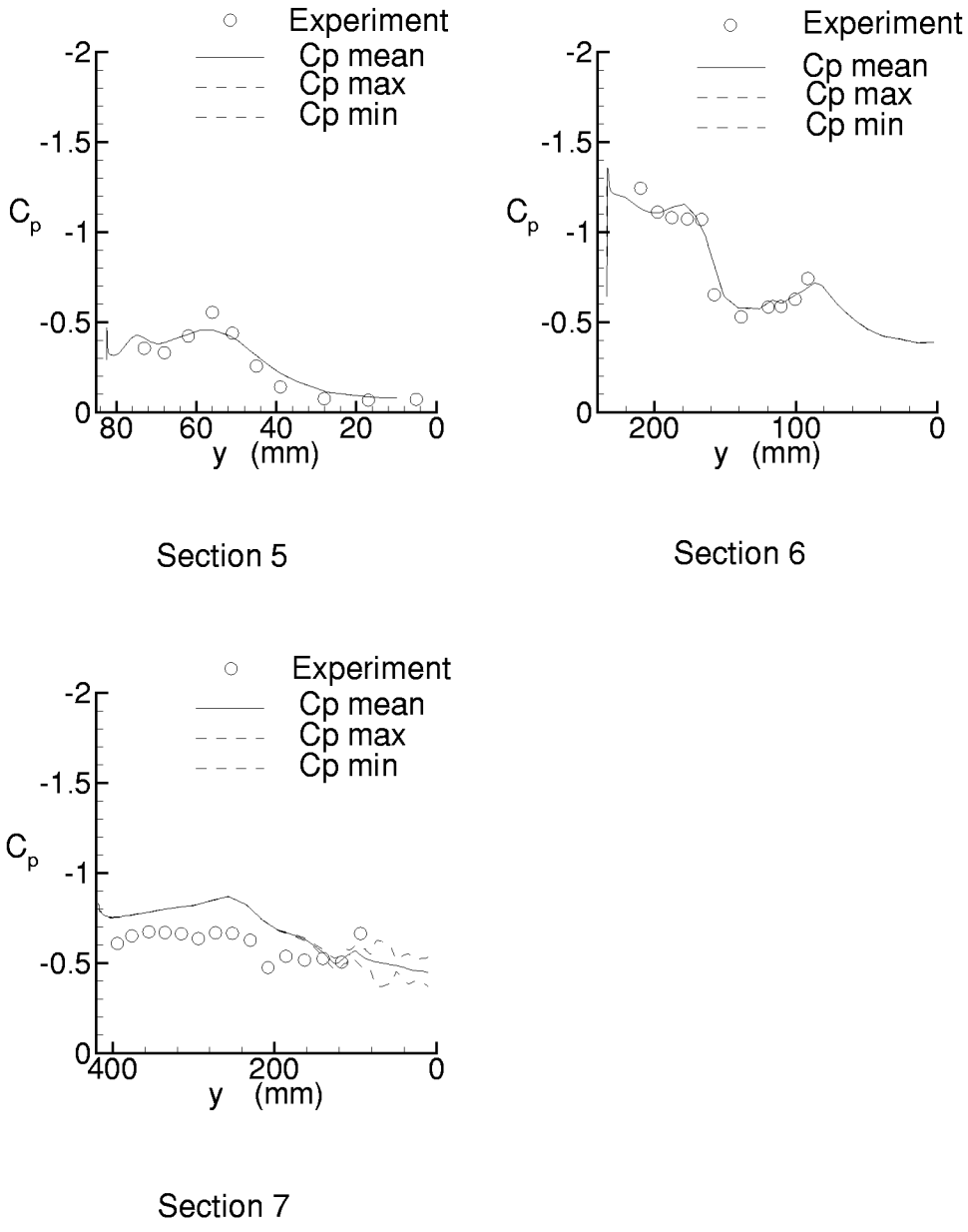

Figure 10. Spanwise unsteady pressure coefficient distributions at chord sections. M = 0.899, α = 11.39 degrees, Re = 8 million. Spalart-Allmaras model. Transition modeled.

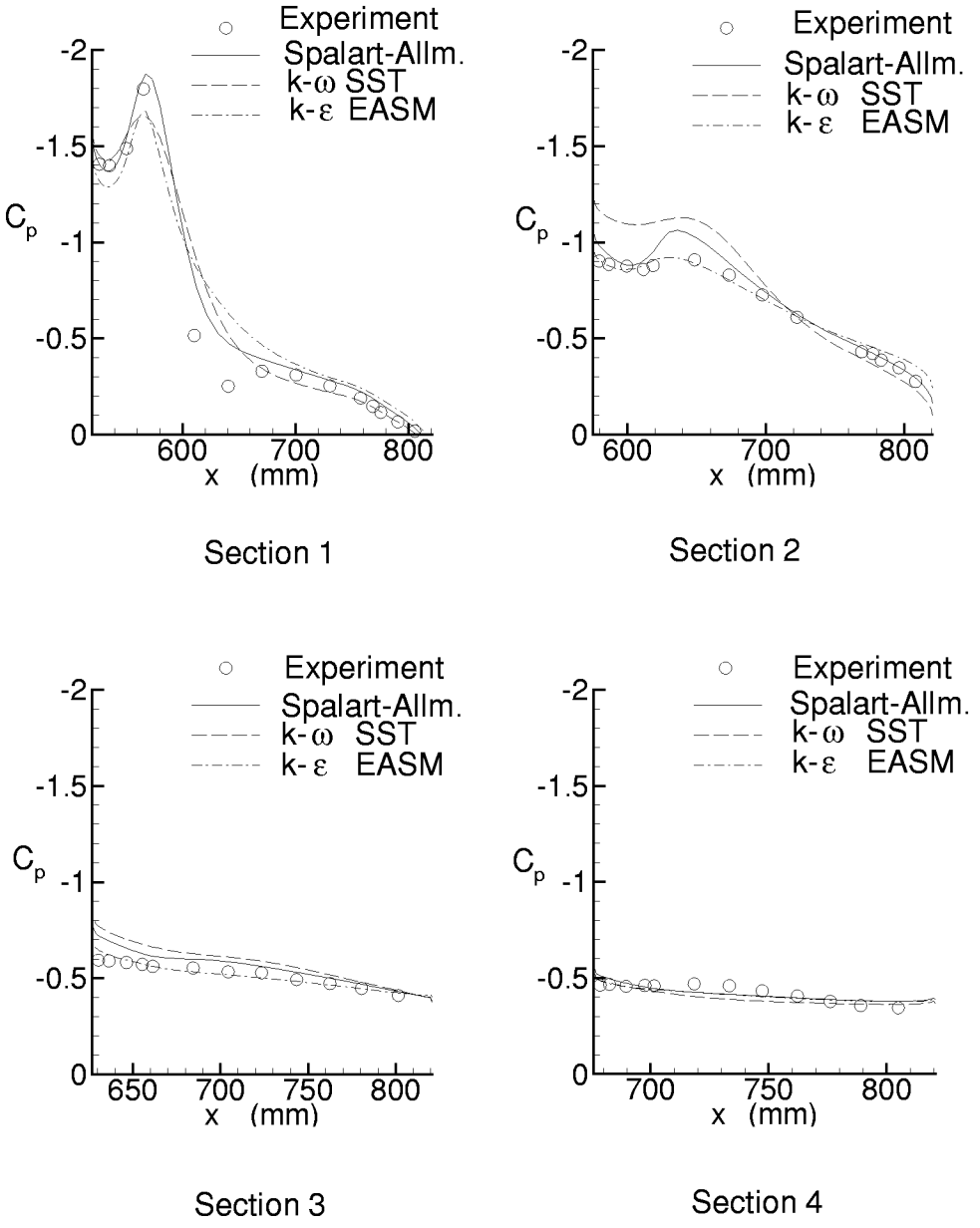

Figure 11. Chord wise pressure coefficient distributions at span sections. M = 0.601, α = 11.94 degrees, Re = 8 million. Transition modeled.

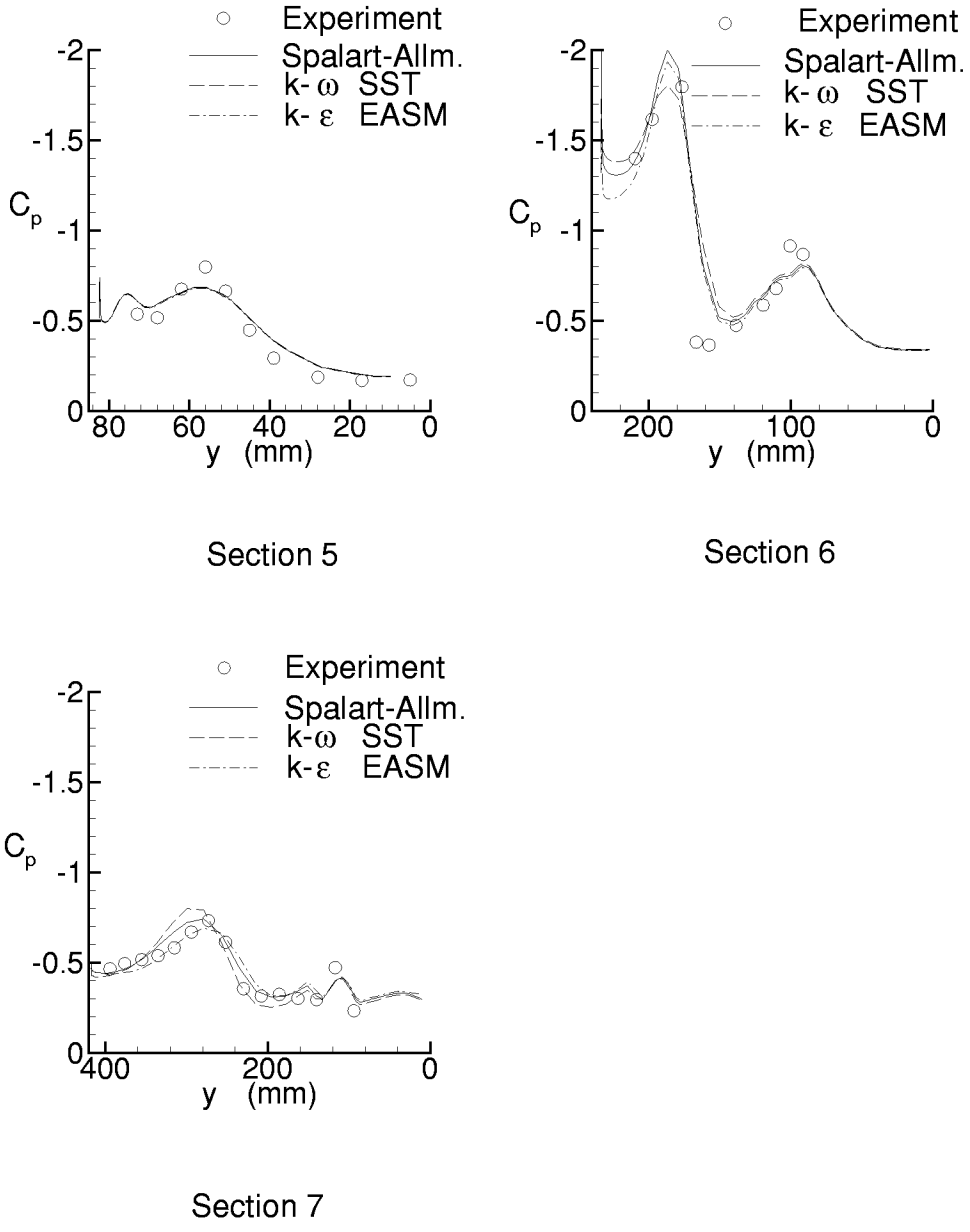

Figure 12. Spanwise pressure coefficient distributions at chord sections. M = 0.601, α = 11.94 degrees, Re = 8 million. Transition modeled.

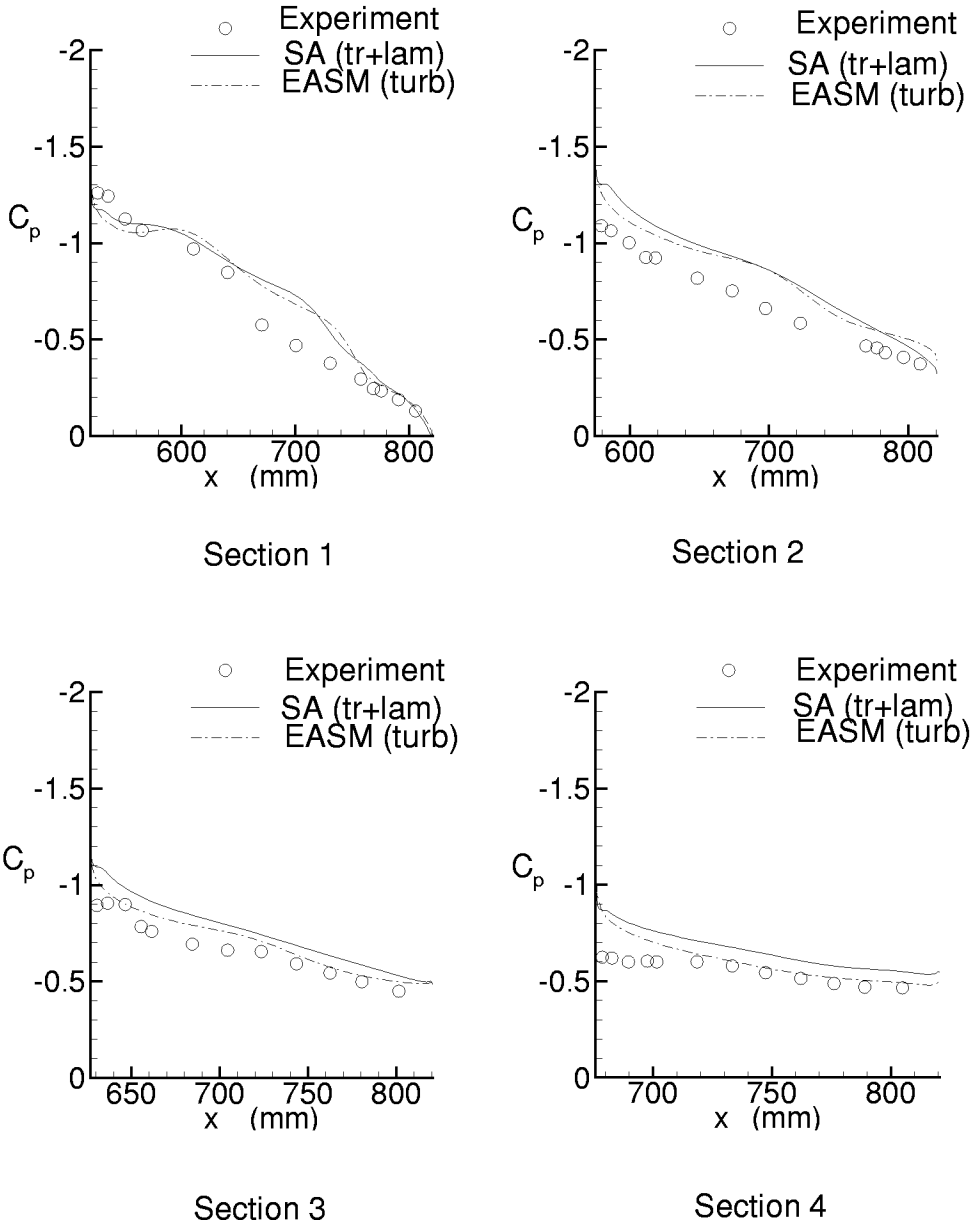

Figure 13. Chord wise pressure coefficient distributions at span sections. M = 0.899, α = 11.39 degrees, Re = 8 million.

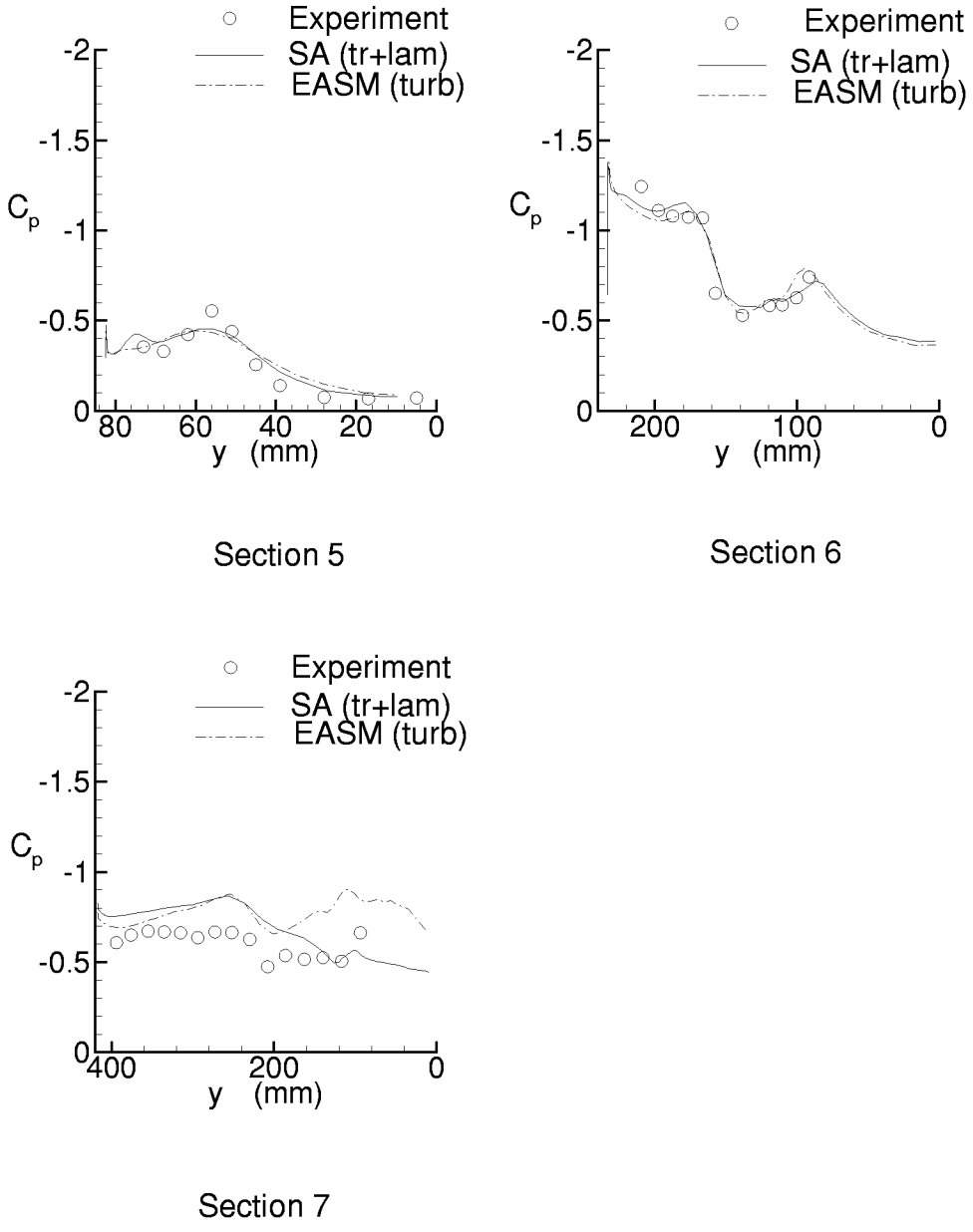

Figure 14. Spanwise pressure coefficient distributions at chord sections. M = 0.899, α = 11.39 degrees, Re = 8 million.

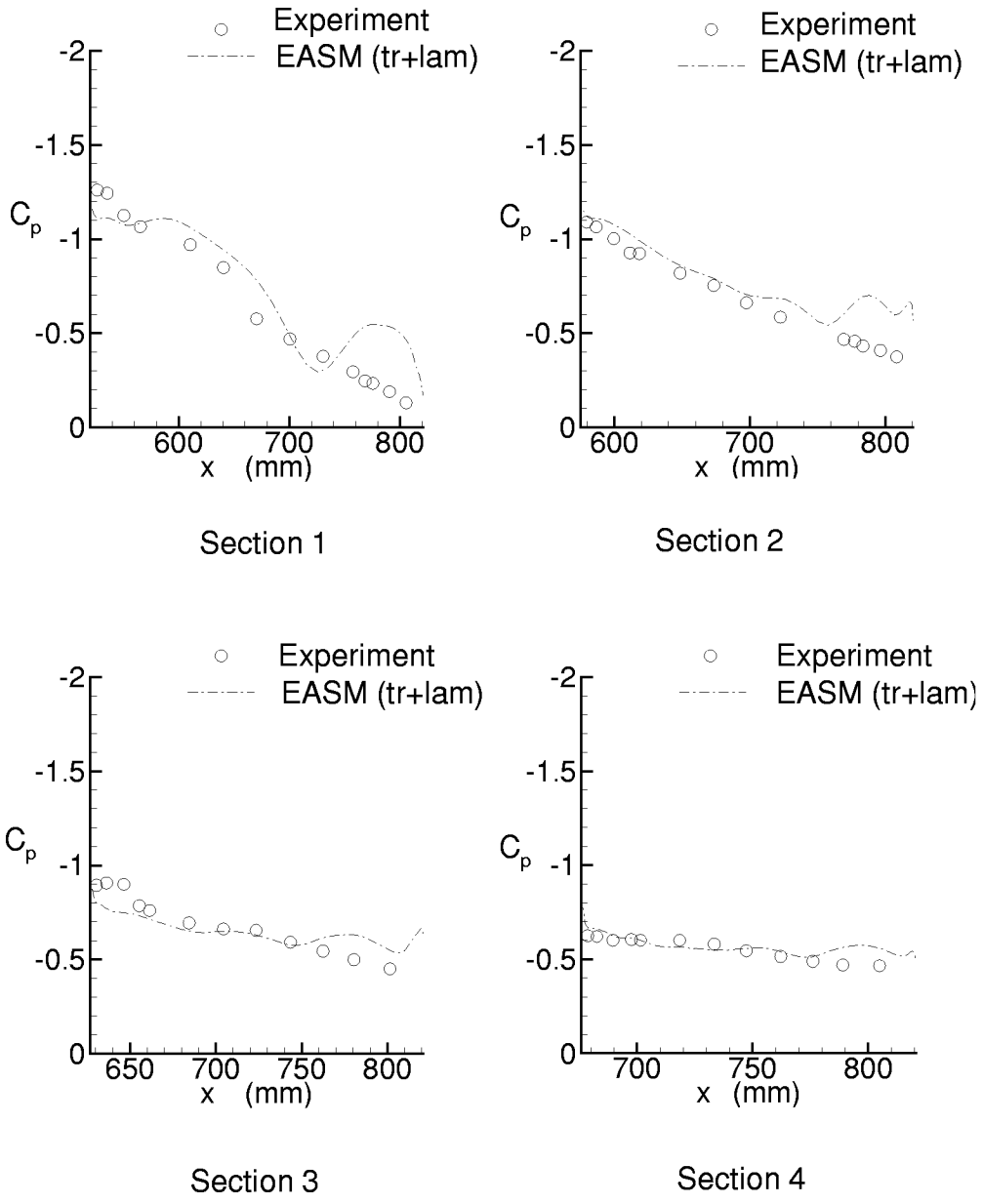

Figure 15. Chord wise pressure coefficient distributions at span sections. M = 0.899, α = 11.39 degrees, Re = 8 million. Transition modeled

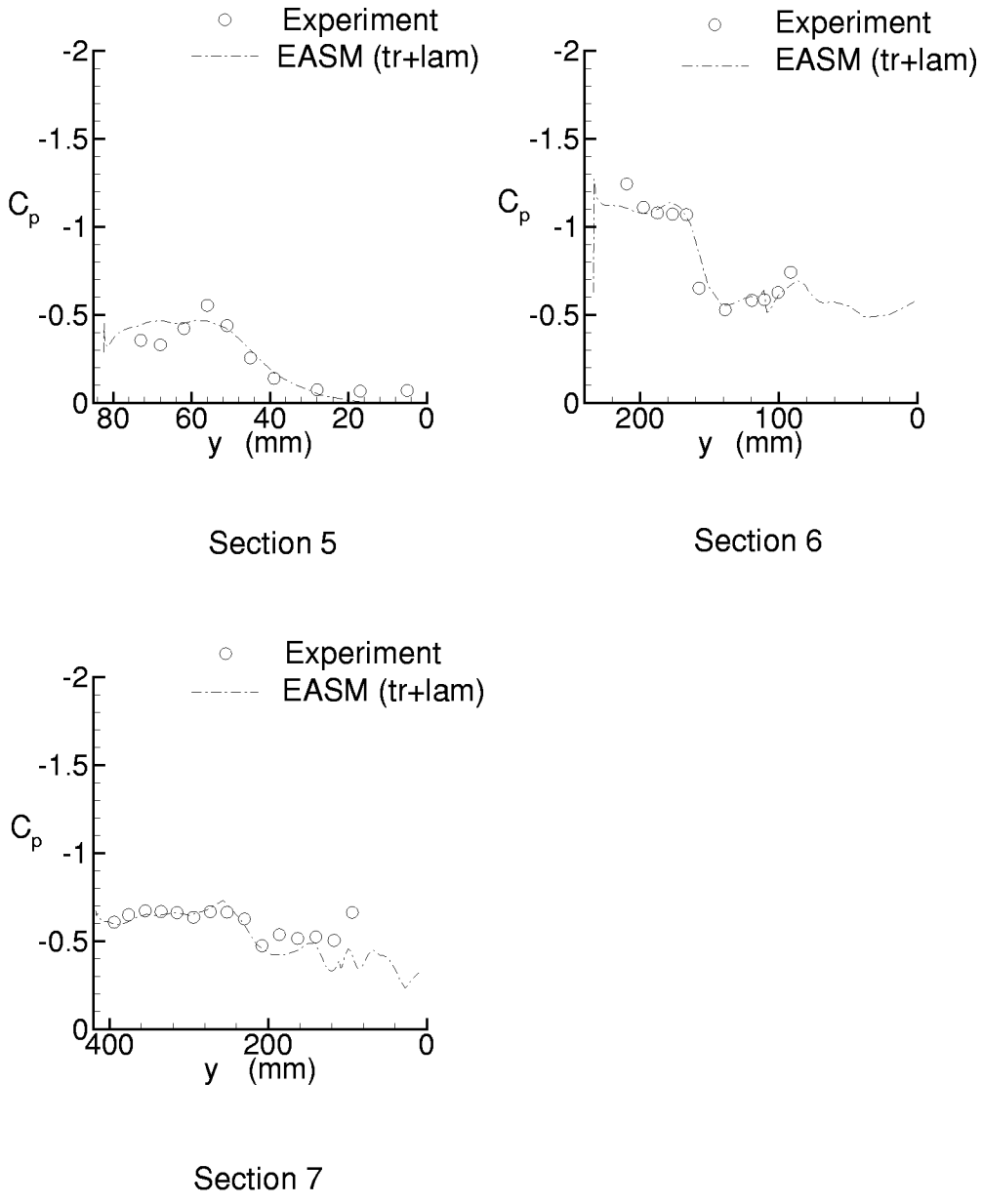

Figure 16. Spanwise pressure coefficient distributions at chord sections. M = 0.899, α = 11.39 degrees, Re = 8 million. Transition modeled

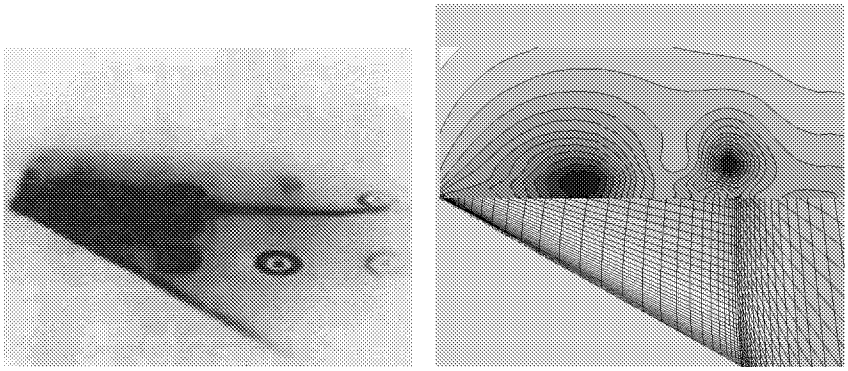

a) Experiment (sheet 9) b) EASM model

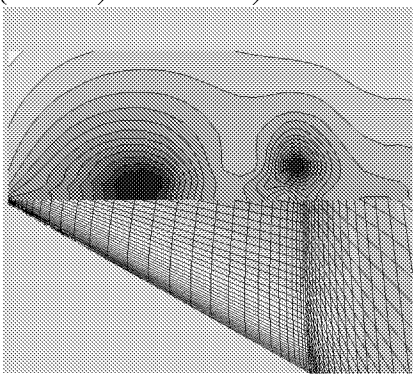

c) Spalart-Allmaras model

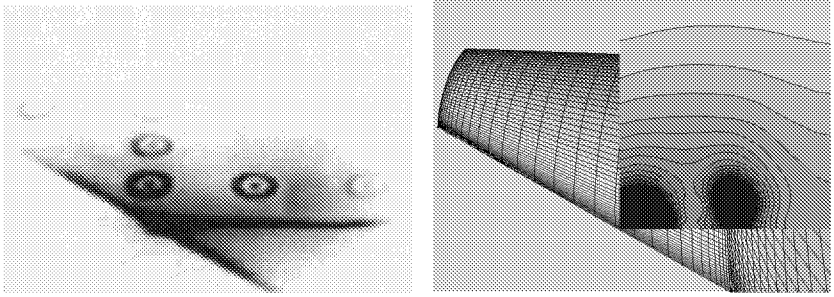

d) Experiment (sheet 8) e) EASM model

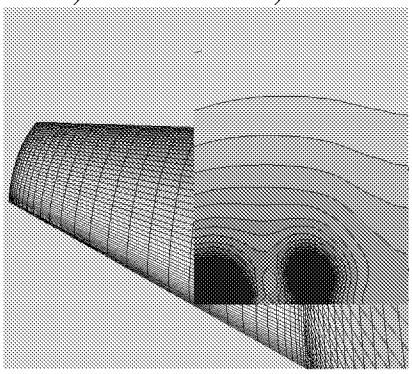

f) Spalart-Allmaras model

Figure 17. Experimental and computed laser light sheet images.
M = 0.601, α = 11.94 degrees, Re = 8 million. Transition modeled.

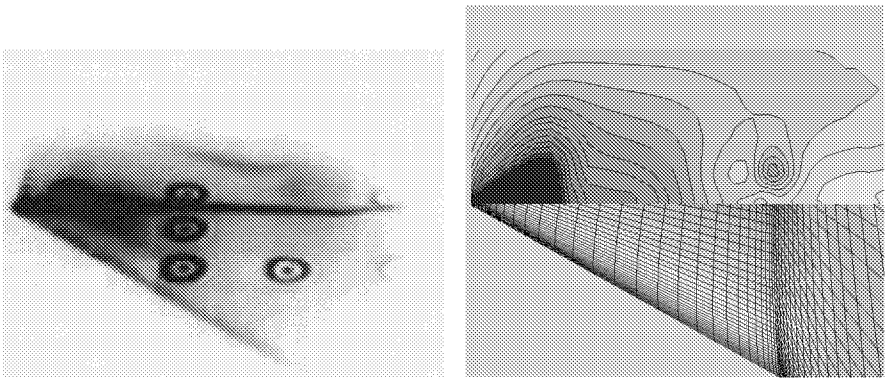

Figure 18. Experimental and computed laser light sheet images.
M = 0.900, α = 9.38 degrees, Re = 8 million. Spalart-Allmaras model.
Transition modeled.

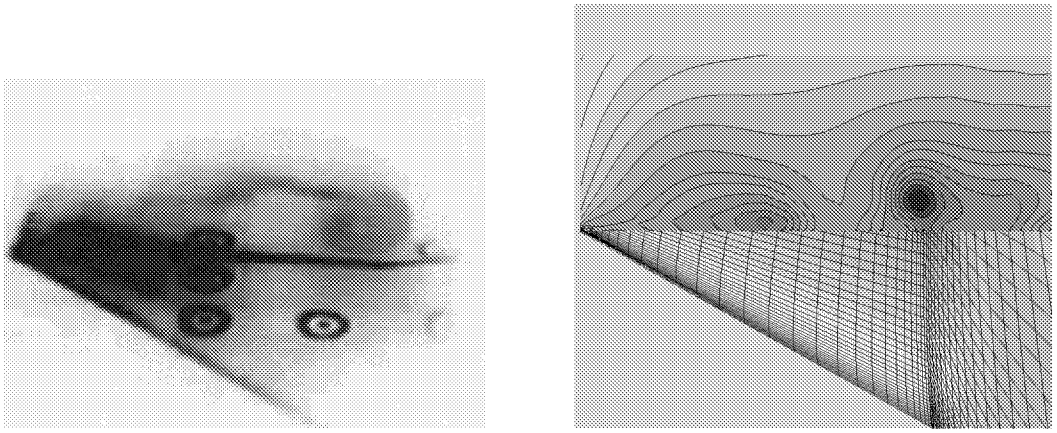

a) Experiment (sheet 9)

b) EASM model (fully turbulent)

c) S-A model (fully turbulent)

d) S-A model (trans., snap shot)

Figure 19. Experimental and computed laser light sheet images.
M = 0.899, α = 11.39 degrees, Re = 8 million.

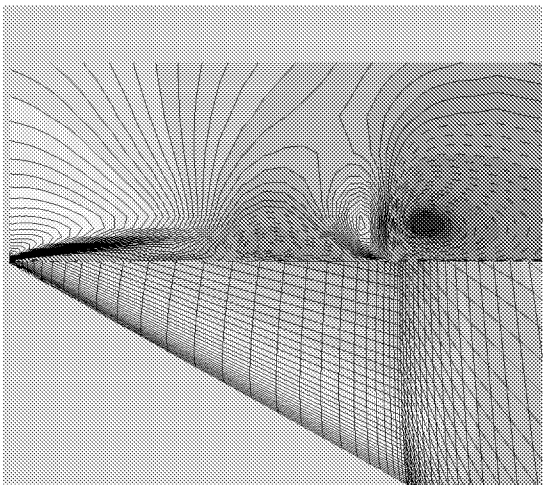

Figure 20. Spanwise flow contours. (dashed lines – tip ward flow)
M = 0.899, α = 11.39 degrees, Re = 8 million. SA, fully turbulent.

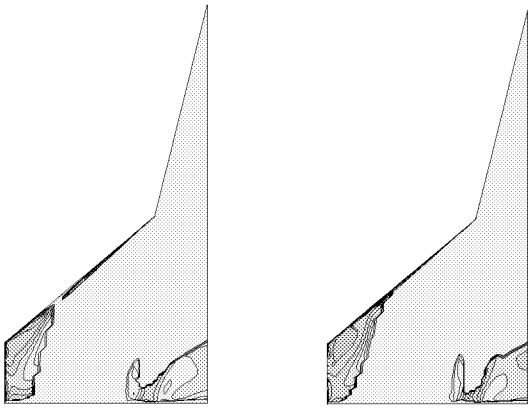

a) Spalart-Allmaras (fully turb) b) k-ω SST (fully turb)

Figure 21. Negative skin friction contours.
M = 0.899, α = 11.39 degrees, Re = 8 million.

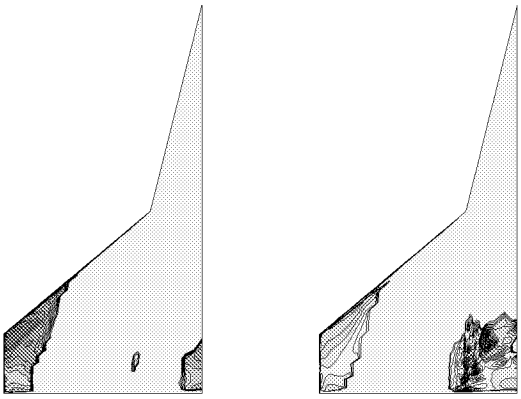

c) k-ε EASM (full turb) d) Spalart-Allmaras (trans)

Figure 21. (Continued) Negative skin friction contours.
M = 0.899, α = 11.39 degrees, Re = 8 million.

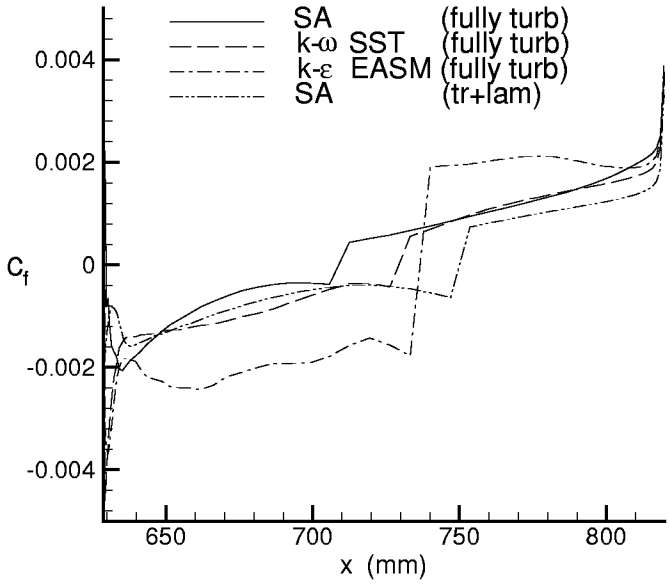

Figure 22. Skin friction coefficient versus x (Section 3).
M = 0.899, α = 11.39 degrees, Re = 8 million.

REPORT DOCUMENTATION PAGE

Form Approved
OMB No. 0704-0188

1. AGENCY USE ONLY (Leave blank)	2. REPORT DATE	3. REPORT TYPE AND DATES COVERED
	May 2000	Technical Memorandum

4. TITLE AND SUBTITLE
Prediction of Transonic Vortex Flows Using Linear and Nonlinear Turbulent Ebby Viscosity Models

5. FUNDING NUMBERS
WU 522-31-21-05

6. AUTHOR(S)
Robert E. Bartels and Thomas B. Gatski

7. PERFORMING ORGANIZATION NAME(S) AND ADDRESS(ES)
NASA Langley Research Center
Hampton, VA 23681-2199

8. PERFORMING ORGANIZATION REPORT NUMBER
L-17986

9. SPONSORING/MONITORING AGENCY NAME(S) AND ADDRESS(ES)
National Aeronautics and Space Administration
Washington, DC 20546-0001

10. SPONSORING/MONITORING AGENCY REPORT NUMBER
NASA/TM-2000-210282

11. SUPPLEMENTARY NOTES

12a. DISTRIBUTION/AVAILABILITY STATEMENT
Unclassified-Unlimited
Subject Category 02 Distribution: Standard
Availability: NASA CASI (301) 621-0390

12b. DISTRIBUTION CODE

13. ABSTRACT (Maximum 200 words)
Three-dimensional transonic flow over a delta wing is investigated with a focus on the effect of transition and influence of turbulence stress anisotropies. The performance of linear eddy viscosity models and an explicit algebraic stress model is assessed at the start of vortex flow, and the results compared with experimental data. To assess the effect of transition location, computations that either fix transition or are fully turbulent are performed. To assess the effect of the turbulent stress anisotropy, comparisons are made between predictions from the algebraic stress model and the linear eddy viscosity models. Both transition location and turbulent stress anisotropy significantly affect the 3D flow field. The most significant effect is found to be the modeling of transition location. At a Mach number of 0.90, the computed solution changes character from steady to unsteady depending on transition onset. Accounting for the anisotropies in the turbulent stresses also considerably impacts the flow, most notably in the outboard region of flow separation.

14. SUBJECT TERMS	15. NUMBER OF PAGES
linear eddy; viscosity models; vortex flow; nonlinear eddy	35
	16. PRICE CODE: A03

17. SECURITY CLASSIFICATION OF REPORT	18. SECURITY CLASSIFICATION OF THIS PAGE	19. SECURITY CLASSIFICATION OF ABSTRACT	20. LIMITATION OF ABSTRACT
Unclassified	Unclassified	Unclassified	UL